Sea-state dependent damping of second-order difference-frequency wave motion of a floating wind turbine with heave plates

J. Orszaghova[1,2], **P.H. Taylor**[1], **H. Wolgamot**[1], **A. Pegalajar-Jurado**[3], **H. Bredmose**[3]
jana.orszaghova@uwa.edu.au
[1] Oceans Graduate School, University of Western Australia, Crawley, WA, Australia
[2] Blue Economy Cooperative Research Centre, Launceston, TAS, Australia
[3] DTU Wind and Energy Systems, Technical University of Denmark, Denmark

HIGHLIGHTS

- Amplitude- and phase-manipulated irregular wave tests are used to gain insight into linear and non-linear responses of a model floating wind turbine.
- We find that the motion response scales linearly with the wave input both in the wave frequency range and surprisingly also for the difference-frequency response at the natural frequencies.
- Amplitude-dependent signal conditioning analysis is applied to show that the resonant slow-drift pitch motions are driven by second-order difference-frequency forcing, but with damping proportional to the sea-state severity.

INTRODUCTION

In contrast to bottom-fixed wind turbines, floating offshore wind turbines can undergo relatively large motions due to wind and wave loads. Pitching is the most important global mode of motion, and can couple with the rotor dynamics and blade pitch control. Here, we examine both linear and low-frequency wave driven motion of a turbine supported on a mostly submerged buoyant frame which is taut-moored.

WAVE BASIN EXPERIMENTS

We report on wave basin experiments carried out in 2021 in the deep water basin at DHI, Hørsholm, Denmark, which is 30 m wide and 20 m long, with water depth of 3 m. The floating structure consisted of a 1:60 scale model of the DTU 10MW reference wind turbine and a variant of the TetraSub floater of Stiesdal Offshore. The floater is made up of a main column connected, through a simple triangular frame, to three sets of buoyancy tanks with heave plates, from which angled taut mooring lines lead to the basin floor (see Fig. 1). The system possesses one plane of symmetry which, in these tests, is aligned along the wave propagation direction.

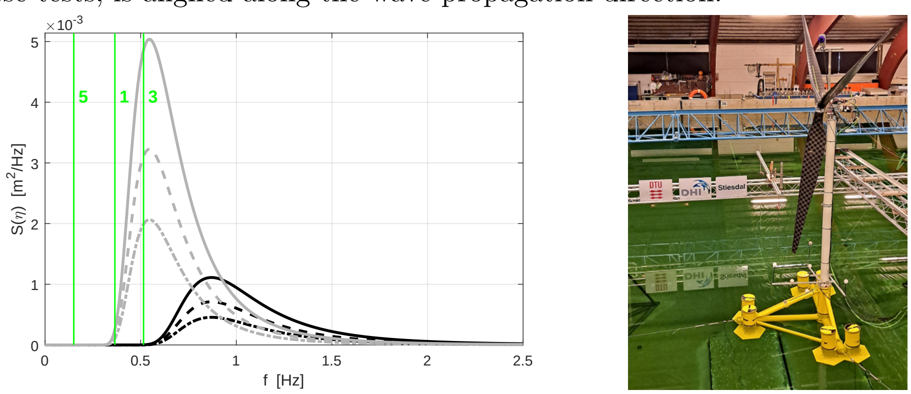

Figure 1: Left: Free surface variance spectra (black and grey lines) together with the rigid body motions natural frequencies (green lines). Right: Photograph of the model in the basin.

We consider two long-crested sea-states with peak periods T_p of 14.2 and 8.9 s (1.83 and 1.15 s in model scale), which we refer to as the long and the short period sea-states. Each spectral shape was created in the basin with three different levels of excitation: the nominal significant wave height

H_s as well as reduced severity sea-states with $0.8 \times H_s$ and $0.64 \times H_s$. The nominal H_s values were 10.5 m and 6.2 m for the long and the short period sea-states respectively (corresponding model scale values of 0.175 and 0.103 m). Additionally, in order to allow for separation of individual harmonics in post-processing, two phase-manipulated tests were carried out for each condition: the original run with random phases and an inverted run with each Fourier component phase-shifted by π rad (simply achieved by inverting the original linear wavemaker command signal). The duration of each of these irregular runs was 1500 s, corresponding to roughly 800 and 1300 waves for the long and the short T_p conditions. In this work, no wind loading is considered, with the turbine idled and the rotor inactive during the tests. We analyse rigid body motions (denoted by 1, 3 and 5 for surge, heave and pitch). As seen in Fig 1, we note that the taut mooring system increases the natural frequencies above those for the unrestrained and/or soft-moored floater, such that the surge and heave frequencies lie within the linear excitation range of the long period sea-state.

LINEAR AND APPROXIMATE QUADRATIC TRANSFER FUNCTIONS

We first analyse the motion response in the frequency domain, through reconstruction of linear and approximate quadratic transfer functions in the linear and sub-harmonic frequency range. Considering each pair of phase-manipulated runs, the measured timeseries are processed together: addition of the signals retains the even harmonic content, while subtraction gives the odd harmonics (see e.g. [1]). The motion signals $x(t)$ and the synchronous measurements from a wave gauge laterally offset from the model $\eta(t)$, representative of the undisturbed free surface, are processed in this way. The odd and even harmonics spectra are shown in Fig. 2, where considerable slow-drift resonant motions (solid lines) can be seen in addition to linearly driven responses (dash-dotted lines). We note the heave-pitch coupling with significant heave motion at the pitch natural frequency.

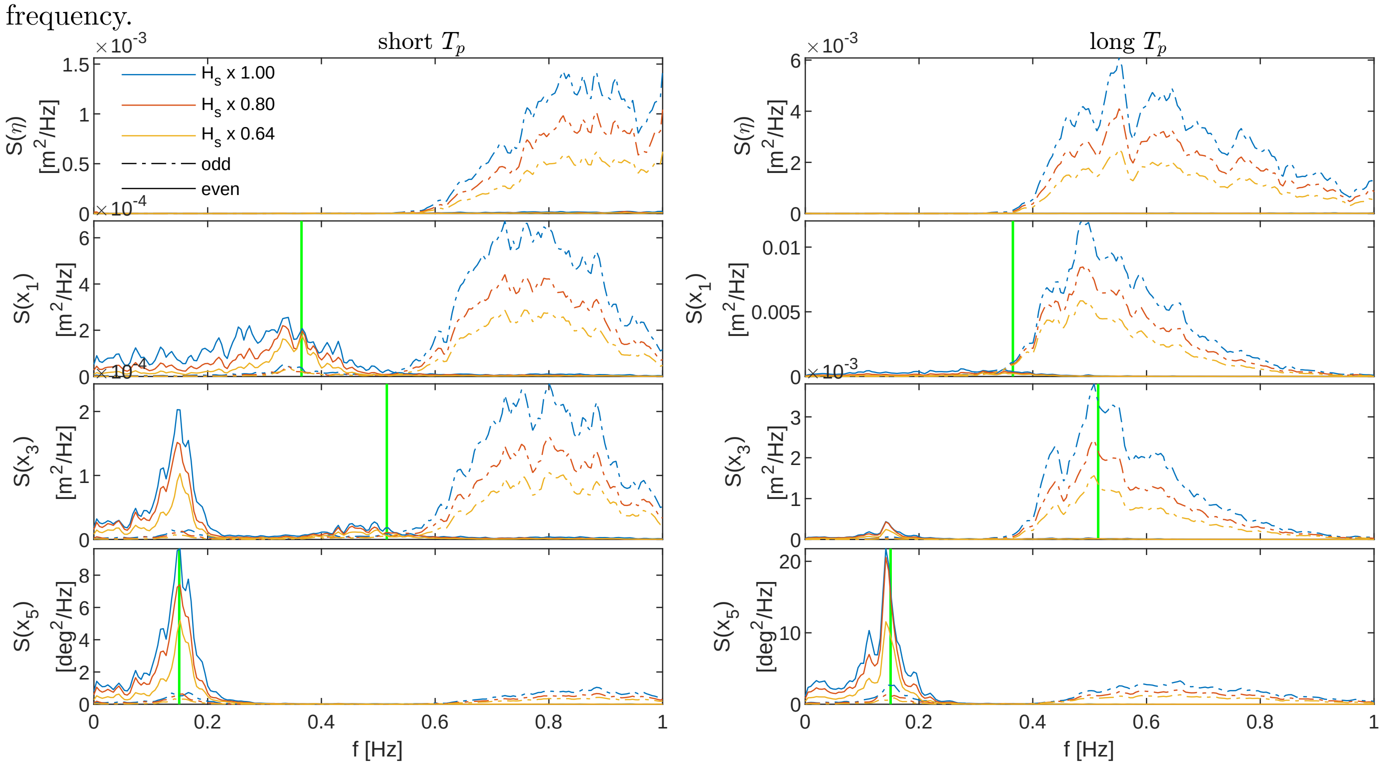

Figure 2: Free surface and motion responses variance spectra.

Band-pass filtering is used to isolate the linear terms, which are used to calculate the linear transfer functions LTF from waves to motions, as per Eq. 1. As shown in Fig. 3, for each mode, the LTFs from different (H_s, T_p) conditions largely collapse onto a single curve. The resonant heave motions appear to behave linearly suggesting that radiation damping is dominant.

To investigate the slow-drift even-harmonic responses, we calculate a simplified quadratic transfer function $\overline{QTF}$ (see e.g. [2] and [3]), which we define as the ratio of the complex amplitudes of the second-harmonic motions and of the square of the linearised free surface, as per Eq. 1. For the slow-drift motions, we simply consider the sub-harmonic frequency range.

$$LTF = \frac{\hat{x}^{(1)}}{\hat{\eta}^{(1)}} \qquad \overline{QTF} = \frac{\hat{x}^{(2)}}{[\hat{\eta}^{(1)}]^2} \tag{1}$$

The linearised free surface raised to the n^{th} power is a proxy for the n^{th} order forcing, which at second-order is due to contributions from products of two linear processes as well as scattering of the second-order incident wave field. The simplified $\overline{QTF}$s thus represent a ratio of second-order response to approximate second-order forcing given as a function of the output sum/difference frequency. From Fig. 3, for each period sea-state, the three $\overline{QTF}$ curves diverge in the vicinity of the natural frequencies but appear to collapse on top of each other away from resonance. Such behaviour is indicative of variable damping across the scaled H_s runs, as also in e.g. [4] and [5].

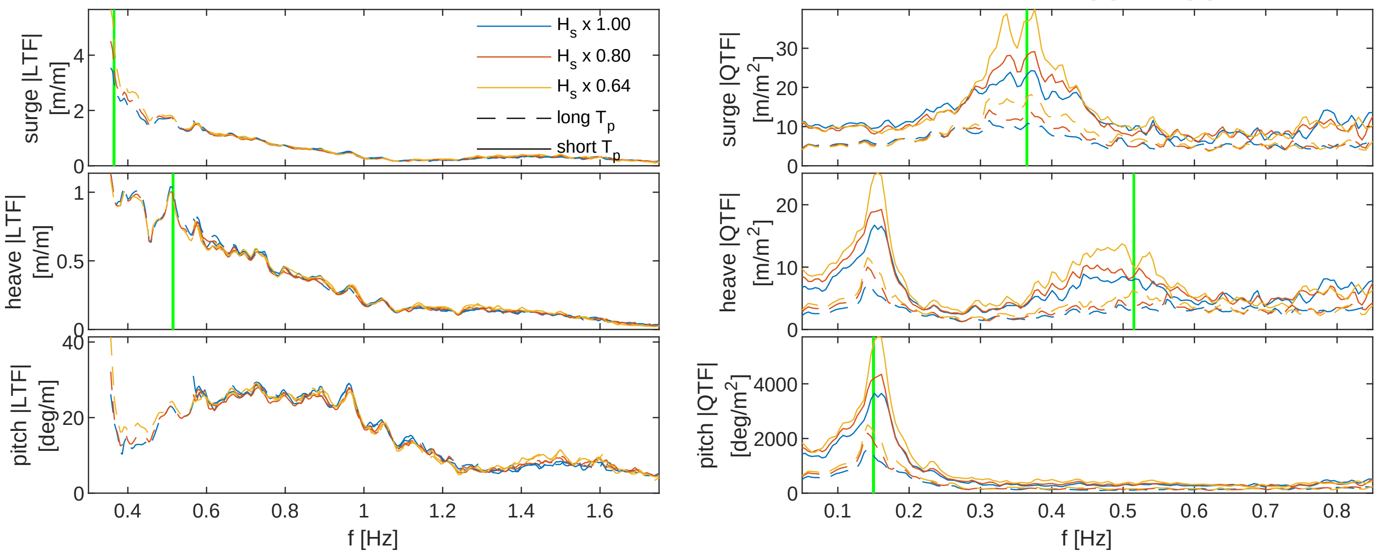

Figure 3: Modulus of the linear and approximate difference-frequency quadratic transfer functions.

AMPLITUDE-DEPENDENT SIGNAL CONDITIONING ANALYSIS

We analyse the resonant even-harmonic response and associated damping by signal conditioning and amplitude dependence analysis, as in [6]. We select a number (here 30) of large events in the conditioning signal, as well as the corresponding sections of the conditioned signal. For each (H_s, T_p) combination, we confirm linear coupling between the resonant second-order sub-harmonic motions and the $[\eta^{(1)}]^2$ proxy through reciprocity (see [7] for derivation). Fig. 4 displays the reciprocity plot for sub-harmonic even pitch response in the short period sea-state. We further examine these correlations at different response and forcing amplitudes. Rather than averaging across the top 30 events as above, we split the data into groups of 20, such that events 1-20 form the first group, events 2-21 the second, etc. We then extract representative amplitudes associated with each group, by simply taking the maxima of the averaged (over 20 events) conditioning and conditioned signals. The correlated extracted amplitudes are plotted in Fig. 4, for conditioning on the response as well as on the forcing proxy. The linear trend, as highlighted by the best fit lines forced to go through the origin, is a further proof of second-order hydrodynamic processes governing the even resonant pitch motions. However, the different slopes across the scaled H_s sea-states suggest that nominally identical wave groups give different levels of resonant response depending on the sea-state they are embedded in. We speculate that, at the low pitch natural frequency, linear radiation damping is small and viscous damping dominates. Using the Morison drag relative velocity formulation, one can approximate the total drag force as a pure forcing/excitation term and a pure linear damping term, with the damping force proportional to $|u_f|u_s$, where u_f and u_s are the fluid and structure velocities (see e.g. [4]). The fluid velocity u_f averaged over the slow resonant response timescales should be proportional to the underlying H_s. This suggests that linear damping of the low-period resonant motions scales with H_s, and the resonant response amplitudes are thus inversely proportional to H_s. To probe this, we scale the extracted response amplitudes from the reduced H_s runs by the H_s fraction (and a constant, here 1.12 in all four cases) to produce the + markers in Fig. 4. The collapse onto a single line is encouraging. The structure 'feels' the background wave-field such that a comparable level of local excitation would result in larger resonant responses in small H_s sea-states and reduced responses in more severe sea-states. This explains the apparent linear scaling of the resonant difference-frequency pitch motion and points at the need for a sea-state dependent damping model for engineering applications.

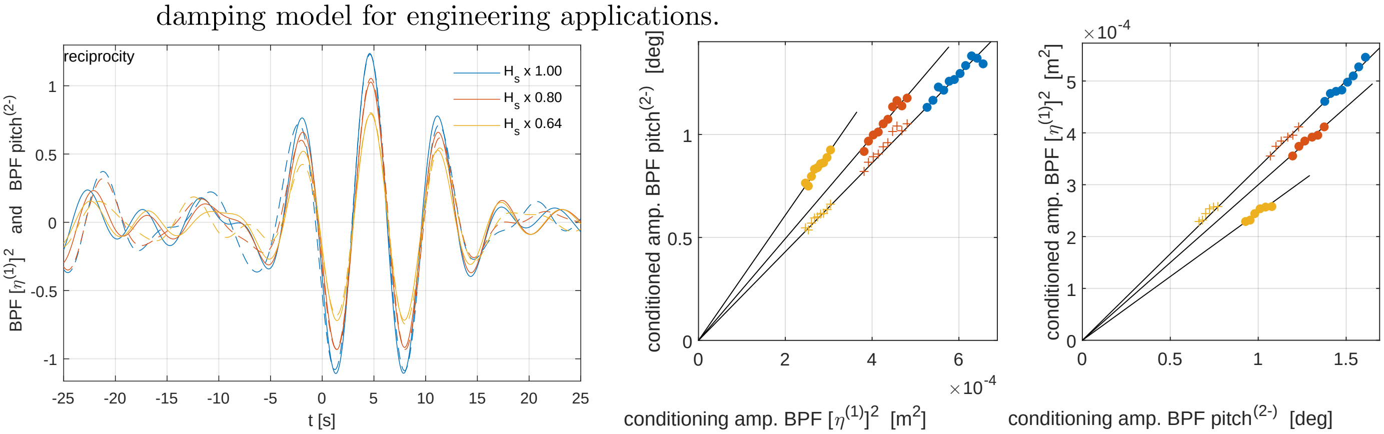

Figure 4: Second-order sub-harmonic pitch motion in the short period sea-state. Left: Reciprocity plot of the conditioned signal analysis. Middle and right: Amplitude dependence analysis. BPF stands for band-pass filtering, here around the pitch natural frequency and applied to both the even-harmonic response and the forcing proxy signals.

ACKNOWLEDGMENTS

This research was supported by Innovation Fund Denmark as part of the FloatStep project (grant no. 8055-00075A). JO and HW also acknowledge support from the UWA Research Priorities Fund, the UWA Research Impact Grant, the Australian Research Council (ARC) Linkage Project LP210100397 and the Blue Economy Cooperative Research Centre (grant no. CRC-20180101). HW is supported by the ARC Early Career Fellowship DE200101478.

REFERENCES

[1] Fitzgerald, C., Taylor, P., Eatock Taylor, R., Grice, J., and Zang, J. 2014. *Phase manipulation and the harmonic components of ringing forces on a surface-piercing column. Proc. of the Royal Society A 470*, 20130847.

[2] Taylor, P. H., Zang, J., Walker, D. A. G., and Eatock Taylor, R. 2007. *Second order near-trapping for multi-column structures and near-flat QTFs.* The 22nd IWWWFB, 1–4.

[3] Zhao, W., Taylor, P., Wolgamot, H., and Eatock Taylor, R. 2021. *Gap resonance from linear to quartic wave excitation and the structure of nonlinear transfer functions. J. of Fluid Mechanics 926*, A3.

[4] Pegalajar-Jurado, A., and Bredmose, H. 2019. *Reproduction of slow-drift motions of a floating wind turbine using second-order hydrodynamics and Operational Modal Analysis. Marine Structures 66*, 178–196.

[5] Pegalajar-Jurado, A., Madsen, F. J., and Bredmose, H. 2019. *Damping identification of the TetraSpar floater in two configurations with Operational Modal Analysis.* ASME 2019 2nd Int. Offshore Wind Technical Conference.

[6] Orszaghova, J., Taylor, P. H., Wolgamot, H. A., Madsen, F. J., Pegalajar-Jurado, A. M., and Bredmose, H. 2021. *Wave- and drag-driven subharmonic responses of a floating wind turbine. J. of Fluid Mechanics 929*, A32.

[7] Zhao, W., Taylor, P. H., Wolgamot, H. A., and Eatock Taylor, R. 2018. *Identifying linear and nonlinear coupling between fluid sloshing in tanks, roll of a barge and external free-surface waves. J. of Fluid Mechanics 844*, 403–434.